Catalytic Significance of the Specificity of Divalent Cations as K_S* and k_{cat}* Cofactors for Secreted Phospholipase A_2[†]

Bao-Zhu Yu,[‡] Joseph Rogers,[‡] Gordon R. Nicol,[‡] Klaus H. Theopold,[‡] K. Seshadri,[§] S. Vishweshwara,[§] and Mahendra Kumar Jain*[,‡]

Department of Chemistry and Biochemistry, University of Delaware, Newark, Delaware 19716, and Molecular Biophysics Unit, Indian Institute of Science, Bangalore 560012, India

Received November 21, 1997; Revised Manuscript Received June 30, 1998

ABSTRACT: Calcium is required for the substrate binding and for the chemical step of the interfacial catalytic turnover cycle of pancreatic phospholipase A_2 (PLA2), but not for the binding of the enzyme to the interface. The role of calcium and other divalent cations (C) is analyzed for the effect on the substrate binding and k_{cat}* for the chemical step. The cofactor role of 3d-cations(II) (C) for the hydrolysis of dimyristoylphosphatidylmethanol (DMPM) vesicles is characterized as an equilibrium dissociation constant for the interfacial binary (E*C) and ternary (E*CL) complexes of PLA2 and substrate mimics (L). Of the cations(II) that promote the binding of a mimic to the enzyme at the interface (E*), only a subgroup supports the chemical step. For example, Cd, Zn, and Cu form ternary E*CL complexes with k_{cat}* of <1 s^{-1}, compared to the rate of >100 s^{-1} with Ca, Fe, Mn, Co, and Ni. Oxygen exchange from $H_2{}^{18}O$ to the products of hydrolysis of DMPM incorporates one ^{18}O in myristate. Incorporation of the first and second ^{18}O occurs during the incubation of both the products of hydrolysis in $H_2{}^{18}O$ with PLA2 and Ca, but not with Zn. The cation-dependent changes in the UV difference spectrum, associated with the formation of E*C and E*CL, suggest that the changes are mainly due to catalytic His-48, and possibly Tyr-52 and Tyr-73, and are different with Ca as opposed to Zn. These results and simulations suggest considerable plasticity in the calcium binding and catalytic site environment. It is proposed that the higher ground state stability of the E*CS complex with the inhibitory cations increases the effective activation energy. For the chemical step, calcium coordinated with a nucleophilic water and the ester carbonyl oxygen facilitates the near-attack geometry in the E*CaS, and the His-48·Asp-99 pair acts as a proton acceptor. As a prelude to establishing the catalytic mechanism, factors controlling the energetically demanding transition state are also discussed.

Calcium is a cofactor for the catalysis by secreted 14 kDa phospholipase A_2 (PLA2)[1] (*1*−*3*). As a part of the highly conserved active site (Figure 1A), calcium is present in a pentagonal bipyramidal first coordination shell (Figure 1B) formed by seven oxygen ligands (*4*−*9*). In pancreatic PLA2, two equatorial bidentate ligands are from the carboxylate of Asp-49, and three other ligands are from the backbone carbonyl oxygen of highly conserved Tyr-28 (axial or apical), Gly-30 (equatorial), and Gly-32 (equatorial) residues. The five ligands provided by the protein are a part of the helix−loop−helix (EF hand) motif in which calcium is exposed to the active site pocket from one side. In the free enzyme, two other ligands are water molecules: W12 in the apical position and W5 in the equatorial position. In addition, there are several other water molecules in the "second shell"; W6 connects W5 to δNH of the His-48·Asp-99 catalytic diad, and W7 is also within 4 Å of W12, W6, and the diad. In cocrystals of PLA2 with substrate mimics, the pentagonal bipyramidal geometry is retained, yet W5 is replaced by the oxygen of the *sn*-2-carbonyl or an equivalent substituent, and W12 is replaced by the *pro-S* oxygen of the *sn*-3-phosphate in the mimic (*10*, *11*) as also suggested by studies with chiral thiophosphate analogues of the substrate (*12*). On the other hand, in the complex of PLA2 with MJ33, a *sn*-2-tetrahedral mimic without a *sn*-3-phosphoester group of the substrate, calcium is six-coordinated with pentagonal monopyramidal geometry (*9*). The *sn*-3-phosphate of substrate is not

[†] This work was supported by U.S. Public Health Service Grant GM29703. The hospitality of the Nehru Center during the visits of M.K.J. to Bangalore is gratefully acknowledged.

[‡] University of Delaware.

[§] Indian Institute of Science. Current address: INBRI, Bangalore, India.

[1] Abbreviations: AM3, 6,9,12-linolenoylamide; BAPTA, 1,2-bis-(*O*-aminophenoxy)ethane-*N*,*N*,*N*′,*N*′-tetraacetic acid; DC_7PC, 1,2-diheptanoyl-*sn*-glycero-3-phosphocholine; DC_8PX, 1,2-dioctanoyl-*sn*-glycero-3-X (where As is arsonate, PA phosphatidic acid, PM phosphomethanol, and PhM phosphonomethanol); deoxy-LPC, 1-hexadecylpropanediol-3-phosphocholine; dithio-DMPM, 1,2-dimyristoyl-1,2-dithio-*sn*-glycero-3-phosphomethanol; DMPC, 1,2-dimyristoyl-*sn*-glycero-3-phosphocholine; DMPM, 1,2-dimyristoyl-*sn*-glycero-3-phosphomethanol; DTPC, 1,2-ditetradecyl-*sn*-glycero-3-phosphocholine; DTPM, 1,2-ditetradecyl-*sn*-glycero-3-phosphomethanol; LPM, 1-myristoyl-*sn*-glycero-3-phosphomethanol; MA, myristate; MG14, 1-octyl-2-(phosphonoheptyl)-*sn*-glycero-3-phosphoethanolamine; MJ33, 1-hexadecyl-3-(trifluoroethyl)-*rac*-glycero-2-phosphomethanol; PLA2, phospholipase A_2 from pig pancreas unless indicated otherwise; Quin-2, 2-[[2,2-bis(carboxymethyl)amino-5-methylphenoxyl]methyl]-6-methoxy-8,8-bis(carboxymethyl)aminoquinoline; RM2, 1-thiooctadecyl-2-acetamido-*sn*-glycero-3-phosphocholine; T*, tetrahedral-like transition state or intermediate. All kinetic and equilibrium parameters are defined in Scheme 1.

S0006-2960(97)02860-2 CCC: $15.00
Published on Web 08/15/1998

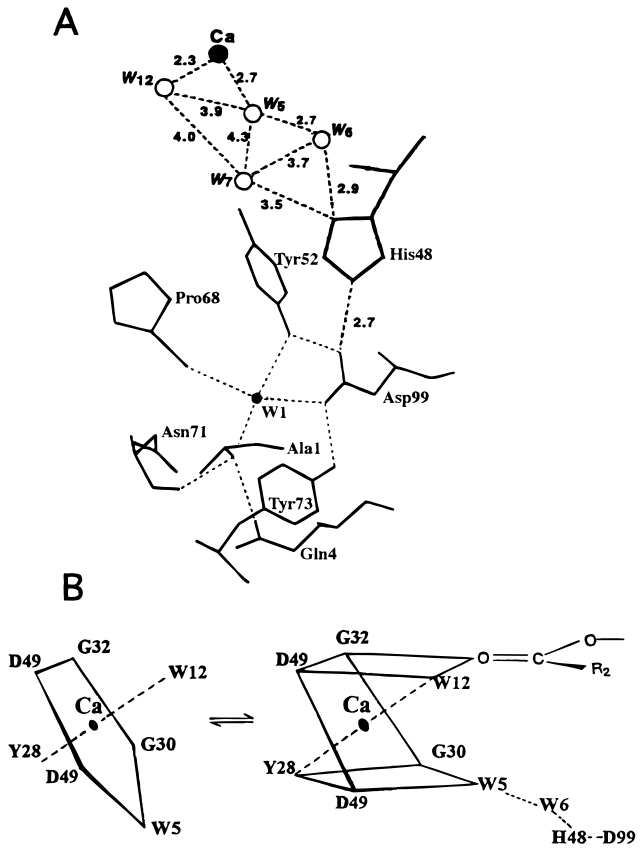

FIGURE 1: (A) Environment of calcium at the catalytic site of pancreatic PLA2 (*3*, *6*, *8*). The numbers represent distances between the heavy atoms (N, C, and Ca). (B) (Left) Pentagonal bipyramid coordination environment and geometry of calcium in the crystal structure of PLA2 and (right) postulated near-attack square antiprismatic environment of calcium on the introduction of the substrate carbonyl as the eighth ligand. W5 in the first coordination shell of the cation is bonded to His-48 through W6.

necessary for the binding to the active site. However, if it is present in the mimic, the conformation of glycero-*sn*-3-phosphate is the same as in aqueous dispersions. Geometrical considerations suggest that coordination numbers five to nine are possible without a change on the position and geometry of the five oxygen ligands provided by the protein, and four if the carboxylate provides only one ligand.

The role of calcium as an obligatory cofactor in the interfacial catalytic turnover by PLA2 is established by kinetic and equilibrium binding studies (*13*). During interfacial catalysis, the species at the interface (here marked with an asterisk) mediate the catalytic turnover according to kinetic Scheme 2 (*13*−*16*). The binding of PLA2 from the aqueous phase to the interface, i.e., the E to E* step, does not require calcium. A structural role for calcium is ruled out because the conformational and structural stability of the native enzyme do not change on the removal of calcium, or in the Asp-49 mutants which do not bind calcium. These mutants are catalytically inert and do not bind substrate mimics, yet bind to the interface (*17*). Calcium is implicated as a k_{cat}* cofactor in the chemical step by the fact that Cd(II) supports the substrate binding but not the catalysis (*12*, *13*).

In this paper, we characterize the role of calcium and other cations(II) in the events of the catalytic turnover cycle (Scheme 1). Several 3d-cations(II) bind to the active site of PLA2. Some (Cu, Zn, and Cd) are K_S* cofactor for the

Scheme 1: Kinetic Model for Binding of Substrate (S) to PLA2 in the Interface (E*) with an Obligatory Requirement for Calcium (*13*−*16*)[a]

$$\begin{array}{ccccc} ECa & \rightleftarrows & E^*Ca + S & \underset{k_{-1}^*}{\overset{k_1^*}{\rightleftarrows}} & E^*CaS \\ \downarrow\uparrow K_{Ca} & & \downarrow\uparrow K_{Ca}^* & & \downarrow\uparrow K_{Ca}^*(S) \\ E & \rightleftarrows & E^* + S & \leftarrow & E^*S\ (?) \end{array} \qquad \begin{array}{c} \\ \overset{k_2^*}{\rightleftarrows} \\ \\ \end{array} \quad E^*Ca + P$$

[a] As an obligatory K_S* cofactor, the binding of calcium to E* is followed by the binding of S or a mimic (L). Dissociation constants K_{Ca}, K_{Ca}*, and K_{Ca}*(S) characterize the stability of ECa, E*Ca, and E*CaS species, respectively. In the text, we consider the general case where calcium is replaced by other cations (C) for the binding of L, such as active site-directed inhibitors (I), or the product of hydrolysis (P), or the ether analogues of the substrate (DTPM). Constants with an asterisk are for the reaction in the interface. Suffixes on the equilibrium constants are modified with C and L. K_C*(L) is the effective dissociation constant for a cation at the subsaturating concentration of a mimic. K_L* is the dissociation constant for a mimic at saturating cation concentrations. and K_L*(C) is the effective dissociation constant for a mimic at subsaturating cation concentrations. K_M* and k_{cat}* are Michaelis constants for the catalytic turnover in the interface. N_S is the number of phospholipid molecules in the outer monolayer of a vesicle. $N_S k_i$ is the apparent second-order rate constant for the catalytic turnover in the interface in the scooting mode. v_o is the turnover number at the maximum possible mole fraction of the substrate ($X_S = 1$). The mole fraction of an inhibitor for a 50% inhibition of v_o is expressed as XI_{50} and that for a 50% decrease in $N_S k_i$ as nI_{50}.

Scheme 2: Dissection of the Chemical Step with a Hypothetical (tetrahedral) Intermediate

$$E^*CS \underset{k_{-f}}{\overset{k_f}{\rightleftarrows}} T^* \underset{k_{-d}}{\overset{k_d}{\rightleftarrows}} E^*CP \underset{k_{-3}}{\overset{k_3}{\rightleftarrows}} E^*C + P\ (= MA + LPM)$$

substrate or mimic binding, but without a measurable k_{cat}*. Others (Fe, Mn, Co, and Ni) support the substrate binding and catalyze the hydrolysis of DMPM vesicles at rates comparable to those seen with calcium. The k_{cat}* cofactor role of a cation(II) is interpreted in terms of a catalytic mechanism (*8*, *18*) shown in Figure 2, in which the water nucleophile in the expanded coordination sphere of the cation may be in a favorable near-attack conformation (Figure 1B).

MATERIALS AND METHODS

Quin-2 and BAPTA were purchased from Molecular Probes (Eugene, OR), and DMPC and DC_8PA were from Avanti Polar Lipids. DMPM, DTPM, DMPG, DMPS, deoxy-LPC, MJ33, dimyristoylglycerosulfate (*19*−*21*), DC_8-PX (*18*), and AM3 (*22*) were synthesized. Sources for the following are gratefully acknowledged: MG14 (M. Gelb, University of Washington, Seattle, WA), RM2 (R. Magolda, DuPont, Wilmington, DE), dithio-DMPM (H. S. Hendrickson, University of Washington, Seattle, WA), WT and mutants of bovine PLA2 (M.-D. Tsai, The Ohio State University, Columbus, OH), mutants of pig PLA2 (H. M. Verheij, State University, Utrecht, The Netherlands), and synovial PLA2 (J. Browning, Biogen, Boston, MA). Salts and other reagents used in this study were analytical grade with >99% purity: $CaCl_2$ (Fisher), $CoCl_2$ and $CdSO_4$ (Merck or Aldrich), $CuSO_4$ and $NiCl_2$ (Fisher), ferrous ammonium sulfate (Baker), and $MnCl_2$, $ZnSO_4$, and $MgCl_2$ (Baker). All measurements were carried out at 23−24 °C and pH 8.0. Uncertainties, based on the standard deviations, in measured values are less than 10%, and up to 30% in the derived parameters obtained from the curve fitting (*13*, *23*).

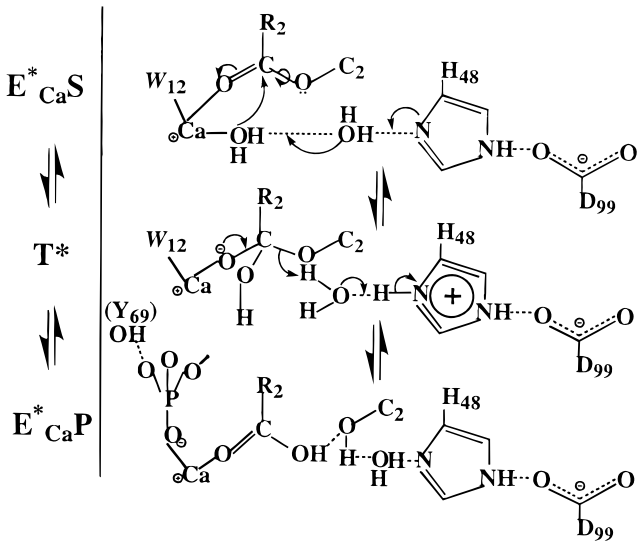

FIGURE 2: Proposed sequence of events during the chemical step of the catalytic cycle of PLA2. It emphasizes a role for the cation cofactor. Several key features of this model are developed in the text. Initial binding of the substrate carbonyl occurs with an expansion of the Ca coordination shell (first step) where W5 could become the nucleophile. Conversion of the substrate tetrahedral intermediate to the one with the product (ES and EP in Scheme 2) is initiated as the oxygen of the *sn*-3-phosphate displaces W12. The rate-limiting transition state is postulated in the second step.

Kinetic and Equilibrium Parameters. All equilibrium and kinetic constants, defined in Scheme 1, were determined as described previously (*13*−*16*, *23*). Detailed studies were carried out with pig pancreatic PLA2, and PLA2 from other sources and site-directed mutants were used for specific purposes. The reaction progress for the hydrolysis of small sonicated vesicles of DMPM was fitted to the integrated interfacial Michaelis−Menten equation to obtain the apparent second-order rate constant, $N_S k_i$ (*14*). The affinity for divalent cations at $X_S = 1$, K_C*(S), was obtained from the dependence of v_o on the divalent ion concentration (*13*). The equilibrium dissociation constants K_C, K_C*, and K_L* were determined by the protection method (*13*, *23*, *24*). Interfacial K_M* values were obtained from a combination of such parameters, including XI_{50} for competitive inhibitors (*13*, *14*, *18*). Inhibition of the zero-order initial rate of hydrolysis of DMPM by Cd(II), Cu(II), and Zn(II) is expressed as IC_{50}, the concentration required for a 50% decrease in v_o at a given calcium concentration.

Kinetic Measurements. Reaction progress was recorded by pH-stat (Radiometer) titration under a stream of nitrogen at pH 8.0 and 23 °C in a 4 mL reaction mixture containing 1 mM NaCl. Before the addition of divalent cation solutions, all salt solutions and buffers were filtered through a column of Chelex (Sigma) to remove trace amounts of multivalent ions. The background concentration of calcium was estimated to be less than 5 μM on the basis of the observed rate of hydrolysis of DMPM in the absence of added Ca(II) or by titration with Quin-2 (described later). Typically, less than 0.1 mL of stock solution of divalent cations was added before adding the substrate, and the reaction mixture was allowed to equilibrate for about 3 min before initiating the reaction progress by PLA2. v_o values at $X_S = 1$ for DMPM vesicles are most conveniently measured in the presence of 20 μg of polymyxin B (*25*) which promotes rapid substrate replenishment through the peptide contact (*26*).

Precautions Necessary for the Kinetic Measurements in the Presence of 3d-Cations(II). Background calcium levels of the solutions without added calcium interfere with the lower-limit estimates of rates in the presence of other cations. Titration with BAPTA or Quin-2 (*27*) with a K_D of <50 nM for calcium was used to estimate these low levels. The limit estimates were necessary for quantifying the cation effects. Controls showed that the probes do not interact with the enzyme. Kinetic effects of cations were characterized in solutions prepared in HPLC grade water. Background rates, which could be totally eliminated by the addition of BAPTA, showed that with such precautions the background calcium concentration in the reaction vessel was variable, largely originating from the anionic lipid samples. Attempts to completely eliminate the background levels of calcium were not entirely satisfactory; however, the levels were routinely reduced to less than 5 μM. Our best method for removing calcium from the lipid solutions included the passage of a methanol solution of phospholipid through a column of CM-Sephadex cation exchanger, which was preconditioned with 0.25 M HCl and then with 4 M NaCl filtered through Chelex and finally equilibrated in methanol.

Complications in the kinetic and equilibrium measurements, due to nonspecific interactions of cations on the anionic substrate interface, could be avoided by using 0.5 mM cations. Cation concentrations were kept below 0.2 mM with dianionic lipids to prevent precipitation and flocculation. The choice of the salt of a cation used for detailed characterization was governed by its stability under the reaction conditions. Around neutral pH, certain metal ions form essentially insoluble hydroxides with solubility products well below 10^{-14} M. Anomalous time-dependent behavior is expected from the hydrolysis of salts and from the rate of precipitation of the hydroxides and oxides. In some cases, such as Fe(II), spontaneous oxidation is also a problem. The observed rates were corrected only if the background drift was less than 20% of the rate; more pronounced drifts were considered intractable.

Analysis of Products of ^{18}O Exchange Reactions by FAB-MS. The product analysis of the PLA2-catalyzed incorporation of ^{18}O from $H_2{}^{18}O$ was carried out by fast atom bombardment mass spectrometry (FAB-MS) on a Micromass AutospecQ apparatus (Manchester, U.K.) equipped with a Cs ion gun. Typically, a sample of lipid dispersion, with other components (Table 7) in buffer with 80 at. % ^{18}O in water, was applied at appropriate time intervals to the FAB probe containing glycerol acidified with HCl as a matrix (*28*). The spectra were obtained in the negative ion mode. The Cs ion voltage was set at 20 kV. The mass range was from 100 to 900 Da.

UV Difference Spectra. Spectra in the 210−360 nm range were recorded on a HP8452 diode array spectrophotometer (Hewlett-Packard) in 10 mM Tris at pH 8.0 and 24 °C with about 10 μM PLA2 in the presence of other additives as indicated in the figure legends. Corrections for dilution, calculation of the difference spectra, and turbidity correction by extrapolation from the baseline in the 325−360 nm region by a monotonic logarithmic function were carried out with the software package provided with the instrument (*32*, *33*). Thus, spectral signatures, characterized as the difference

Table 1: Effect of Cations on the Hydrolysis of DMPM Vesicles by PLA2[a]

cation	radius (Å)	pK_a	v_o (s^{-1})	K_C (μM)	K_C* (μM)	K_C*(DMPM) (μM)	K_C*(DTPM) (μM)	IC_{50} (μM)
Ca(II)	1.20	12.7	300	350	250	100	5	
Mg(II)	0.95	11.4	<1	>2000			>2000	
Mn(II)	1.04	10.7	>30	>500				
Fe(II)	1.00	10.1	>30					
Co(II)	0.96	9.6	130	500	300	140	14	
Ni(II)	0.90	9.4	150	>1000	1000	610	14	
Cu(II)	0.94	7.5	<1	1.5	1.5	0.045	0.12	2.5
Zn(II)	0.96	9.6	<1	1	0.6	0.034	0.027	0.6
Cd(II)	1.07	11.7	<1	160	65	0.5	1	1
Sr(II)	1.35			100	100			680
Ba(II)	1.52			300	300			850

[a] The radii and pK_a values are for the coordination number seven (*74, 75*); some estimates are based on the assumption that the radius increases about 6% as the coordination number increases by one. K_C, K_C*, and K_C*(DTPM) were obtained by the protection method; for the inhibitory cations, K_C*(DMPM) or K_C*(DTPM) was also calculated with eq 2.

spectra in the linear concentration-dependent range, rather than the absolute intensities, are used for comparisons. Due to potential problems from excess turbidity, >0.3 OD at 280 nm, results in the presence of mimics are often not at saturating levels of the neutral diluent. However, the metal ion and inhibitor concentration dependence of the spectral changes is consistent with a two-state equilibrium.

RESULTS

3d-Cations(II) Differ as K_S and k_{cat}* Cofactors for the Hydrolysis of DMPM by PLA2.* The kinetic effects of several 3d-cations(II) are analyzed in terms of the primary constants with established relationships, eqs 1−3 (*13*).

$$IC_{50} = K_C^*(L) + \frac{K_C^*(L)}{K_{Ca}^*(S)}[Ca] \quad (1)$$

$$K_C^*(L) = \frac{K_C^*}{1 + \frac{1}{K_L^*}} \quad (2)$$

$$\frac{v_o}{v_I} = 1 + \left(\frac{1 + \frac{1}{K_I^*}}{1 + \frac{1}{K_M^*}}\right)\left(\frac{X_I}{1 - X_I}\right) \quad (3)$$

For cations that support hydrolysis, the values for the apparent kinetic dissociation constant for the cation, K_C*(DMPM) in column 7 of Table 1, were obtained from the hyperbolic cation concentration dependence of the initial rate of hydrolysis of DMPM at $X_S = 1$ (*13*). For example, at saturating calcium, the initial rate, v_o, is 300 s^{-1}, and K_{Ca}*(DMPM) equals 100 μM. The rate of hydrolysis in the presence of Ni(II) and Co(II) is also significant. The hyperbolic concentration dependence gives a v_o of 130 s^{-1} with a K_{Co}*(DMPM) of 140 μM and a v_o of 150 s^{-1} with a K_{Ni}*(DMPM) of 610 μM (Table 1, column 4). These are limit estimates, because Ni(II) at higher concentrations (>300 μM) produced a modest background drift. Although Fe(II) and Mn(II) also support hydrolysis of DMPM vesicles, detailed analysis could not be carried out at pH 8 due to pH drifts associated with their oxidation, hydrolysis, and precipitation as hydroxides. As a control, the rate of hydrolysis of DMPM by PLA2 is <0.1 s^{-1} in the presence of chelating agents such as EGTA or BAPTA. In the absence of added calcium or a chelating agent, the observed rate was typically 5 s^{-1}, corresponding to about a 1 μM background level of calcium in the reaction mixture. Thus, the effective working range for monitoring the catalytic role of added cations that support catalysis is for rates above 5 s^{-1}.

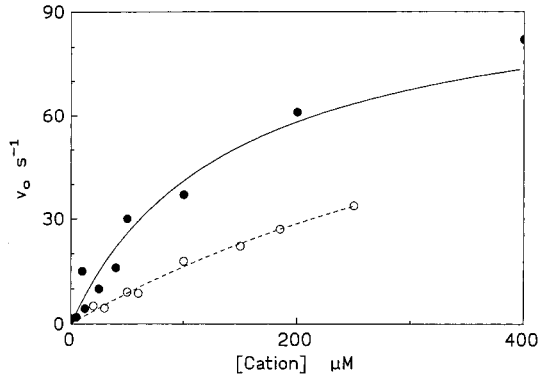

FIGURE 3: Dependence of the initial rate of hydrolysis of DMPM vesicles by pig pancreatic PLA2 on the (●) cobalt(II) or (○) nickel-(II) concentration. The reaction mixture contained DMPM (700 μg or 0.3 mM), polymyxin B (20 μg or 3 μM), and pig PLA_2 (2 pmol) at pH 8.0 and 25 °C in 4 mL of 1 mM Na.

Not all cations(II) that bind to PLA2 support catalysis. Our upper limit estimate is 0.1 s^{-1} for the rates in the presence of Cd, Cu, or Zn in the absence of added calcium. In such cases, K_C*(DMPM) was obtained from competitive inhibition studies (eq 1) and analyzed in terms independently obtained equilibrium constants (eqs 2 and 3). The cation concentration for 50% inhibition of the calcium-mediated hydrolysis of DMPM (IC_{50}, column 9 in Table 1) is obtained as 1/slope from the plot in Figure 4. According to eq 1, IC_{50} is related to K_C*(DMPM) for the dead-end E*C(DMPM) complex. By this criterion, several 3d-cations(II) (Table 1) and 4d-cations(III) (results not shown) compete with calcium for the binding to PLA2, and are potent inhibitors. As shown in Figure 5, IC_{50} for Zn(II) or Cu(II) increases with the calcium concentration. According to eq 1, K_C*(DMPM) is the *y*-intercept in this plot. Since the uncertainty in the value of the *y*-intercept is large, K_C*(DMPM) values in Table 1 (column 7) are calculated from the slope and the kinetically determined K_{Ca}*(DMPM) of 0.1 mM (*13*).

E, E*, and E*L (Table 1) forms have a higher affinity for the inhibitory cations. Dissociation constants K_C and K_C* show a 1000-fold range for the 3d-cations(II). The fact that

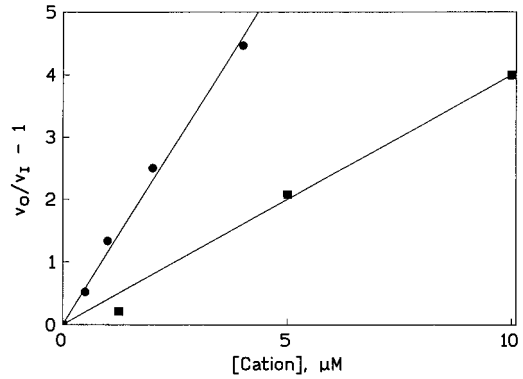

FIGURE 4: Relative rate for the hydrolysis of DMPM in the presence of (●) zinc(II) or (■) copper(II). Addition of the inhibitory cation before or after the initiation of hydrolysis gave identical results. Other conditions were like those described in Figure 3 but with 1 mM Ca.

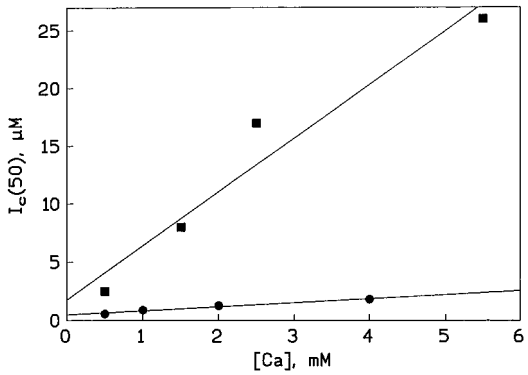

FIGURE 5: Dependence of IC_{50} on [Ca] for (●) Zn(II) or (■) Cu-(II). Other conditions were like those described in Figures 3 and 4.

K_C and K_C* differ by less than a factor of 2 shows that the intrinsic affinity of PLA2 for the neutral diluent remains low irrespective of the nature of the cation, i.e., K_{ND}* > 1 mol fraction (eq 2). K_C*(DTPM) values in column 8 show that all smaller cations except magnesium form stable ternary E*C·DTPM complex. Larger cations such as Ba and Sr, with radii of >1.2 Å (Table 1), bind to E and E*, but do not support the binding of DTPM. Thus, compared to strong dead-end E*C·DMPM complexes formed by Cu and Zn, complexes with Ba and Sr are weaker inhibitors because they form only the weaker EC and E*C complexes, and do not form the ternary complex.

The kinetic K_C*(DMPM) values for the dependence of the rate of hydrolysis are larger than K_C*(DTPM) (Table 1). This is consistent with eq 2, where with K_L* = K_M*(DMPM) = 0.35 mol fraction is larger than K_L* = K_S*(DTPM) = 0.03 mol fraction (*14*, *23*). Also, K_C*(DMPM) values, for the dead-end ternary complex of PLA2 with DMPM and an inhibitory cation, are comparable to the dissociation constant K_C*(DTPM). These values (column 8 in Table 1) were obtained from independently determined K_L* values for DTPM (Table 2). A fair agreement between K_C*(DMPM) and K_C*(DTPM) for Zn, Cu, and Cd shows that these ions do compete with calcium to support the binding of DMPM or DTPM.

The dissociation constant for an inhibitor, K_I*, in the presence of a cation(II) is obtained by the protection method. These values compare favorably with those calculated from the inhibition kinetics (Table 2). According to eq 3, the mole fraction of an inhibitor for 50% inhibition, XI_{50}, is related to K_I* for the inhibitor and K_M* for DMPM obtained by independent methods described in the next subsection (Table 3). Thus, results in Table 2 show that K_L* values for the ternary E*CL complex (L is DTPM, products of DMPM or DMPC, MJ33, MG14, RM2, and AM3) with several cations are comparable; i.e., the affinity for a mimic changes moderately at best with the nature of the cation. When a 30% uncertainty in K_I* values is considered, a 7-fold difference seen with phosphocholine mimics is significant, possibly due to additional cation-dependent interactions with the zwitterionic headgroup.

In short, analysis of the kinetic and equilibrium dissociation constants of cations(II) (Table 1) and mimics (Table 2) in EC, E*C, and E*CL shows that the mimic and substrate binding is supported by all cations, and the change in v_o (Table 1) is attributed to a cation-dependent change in k_{cat}*. Note that the ability of a cation to bind substrate and support catalysis does not depend on its ionic radius or the pK_a of water associated with the cation (columns 2 and 3 in Table 1).

Cobalt and Calcium Are Comparable as K_S and k_{cat}* Cofactors for the Hydrolysis of DMPM.* Results in Table 3

Table 2: Equilibrium Dissociation Constants for Substrate Mimics (mole fraction) for PLA_2 at the Interface in the Presence of Cations

parameter	Ca(II)	Co(II)	Ni(II)	Cu(II)	Zn(II)	Cd(II)
K_L*(DTPM)	0.02	0.03	0.014	0.05	0.04	0.017
K_L*(DTPC)	0.065	0.25		0.26		0.2
K_L*(DC_8PC-ether)	0.1	0.6		0.65		0.54
K_P*(DMPC)	0.02	0.14		0.12		
K_P*(DMPM)	0.03	0.01	0.014	0.02	0.05	0.044
MJ33 K_I* prot.	0.0014	0.004	0.01	0.01	0.01	0.0075
MJ33 K_I* calcd[a]	0.002	0.004	0.008			
XI_{50}	0.006	0.012	0.013			
MG14 K_I* prot.	0.0011	0.004				0.001
MG14 K_I* calc[a]	0.0011	0.022	0.055			
XI_{50}	0.0034	0.06	0.078			
RM2 K_I* prot.	0.0023	0.01				0.003
RM2 K_I* calcd[a]	0.0029	0.0068	0.0056			
XI_{50}	0.009	0.01	0.009			
AM3 XI_{50}	0.006	0.038	0.017			

[a] K_I* values calculated with eq 3 using XI_{50} given in the next row and K_M* from Table 3.

Table 3: Effect of Cations(II) on the Catalytic Parameters of PLA2

parameter	Ca(II)[a]	Co(II)	Ni(II)
v_o (s^{-1})	300	100	>100
$N_S k_i$ (s^{-1})	35	4.3	
nI_{50} for MJ33	0.03	0.03	
ICd_{50} (μM)	1	3.3	
IZn_{50} (μM)	0.6	0.9	
K_M*(DMPM)			
from XI_{50} and K_I*	0.4	0.5	>1.6
from K_P* and $v_o/N_S k_i$	0.36	0.28	
from K_C*(S) and K_C*	0.67	0.88	1.6
from XI_{50} and nI_{50}	0.2		0.44
k_{cat}* (s^{-1})	400	150	250
oxy/thio ratio			
WT (bovine)	10	11	
D99N	4.5	2.8	
D99N/Y52F/Y73F	1.5	2.6	
WT (pig)	10	10	
Y69F	2.5	2.5	

[a] From refs *13*−*15*. The oxy/thio effects were measured with bovine mutants with DMPM and its dithio analogue (*29*).

Table 4: Rates of Hydrolysis of DMPM (v_o in s^{-1}) by PLA2 with Ca(II) or Co(II) as a Cofactor at pH 8 and 23 °C

source	v_o for Ca	v_o for Co
synovial	90	4.5
bee	115	6
bovine		
WT	330	200
K53M	240	200
K56E	230	100
K56M	280	150
I9A	50	50
D99N	20	17
D99N/Y52F/Y73F	11	10
D49E	<0.1	<0.1
pig		
WT	300	105
L31A	270	270
L31R	125	110
L31S	190	40
Y69F	30	27
Y69K	140	110

show that the interfacial catalytic parameters (K_M*, k_{cat}*, and $N_S k_i$) for the hydrolysis of DMPM in the presence of Ca, Co, and Ni are comparable, and so are the $I_{Zn}(50)$ and $I_{Cd}(50)$ values for the inhibition of the hydrolysis of DMPM supported by Ca or Co. The most significant difference is seen in $N_S k_i$, which is consistent (*14*) with lower K_P*(DMPM) (Table 2) and lower k_{cat}* values (see below) in the presence of Co(II). K_M* values for DMPM, obtained by four independent methods, are not significantly different with cobalt or calcium (Table 3). The average K_M* was used to calculate k_{cat}* [$=v_o(1 + K_M^*)$], which is moderately lower with cobalt (Table 3). The oxy/thio ratio of 10 with both Ca and Co suggests that the chemical step remains rate-limiting; i.e., hydrolysis of the thio analogue of DMPM by WT PLA2 proceeds at 10% of the rate seen with DMPM (*29*).

Co(II) Supports DMPM Hydrolysis by Evolutionarily Divergent PLA2. Results in Table 4 show that the cobalt-mediated rates of hydrolysis of DMPM by bovine and pig pancreatic (type I), human synovial (type II), and bee (type III) PLA2 are 5−100% of the rate with Ca. The Ca versus Co discrimination in v_o is unchanged for Lys-53 and Lys-56 mutants with a change in the interfacial recognition region. Mutation of the active site residues in pancreatic PLA2 minimizes the Ca versus Co difference in v_o. Ile-9 and Leu-31, which make contact with the hydrophobic region of the substrate, show an effect that depends on the nature of the substituent. With a change in the cation binding ligand, D49E does not support hydrolysis in the presence of Ca or Co, yet it binds calcium with 10% affinity (*17*).

The oxy/thio (Table 3) and Ca/Co (Table 4) ratio in v_o is lower for D99N and Y69F. As a part of the catalytic diad, a modest effect of D99N mutation on k_{cat}* (*8*) is attributed to a modest change in the stability of the intermediate in the chemical step (Figure 2). The role of Tyr-69 in catalysis (*30*, *76*) is supported by results in Table 5, which show that Y69F is k_{cat}*-impaired with a less than 3-fold change in the equilibrium binding parameters for the cations and mimics. This is particularly significant because the hydroxyl group of Tyr-69 is within H-bond distance of the *pro-R* oxygen of the *sn*-3-phosphate of the *sn*-2-amide analogues (*11*) and the *sn*-2-ester oxygen of MJ33 (*9*). These results imply a weak role for the Tyr-69 hydroxyl in the chemical step.

Table 5: Equilibrium Binding and Catalytic Parameters for Y69F Pig PLA2

parameter	Y69F	WT
inactivation time for E (min)	3.5	2.8
K_L*(deoxy-LPC) mole fraction	0.5	>1
v_o (s^{-1}) for DMPM/Ca	30	300
v_o (s^{-1}) for DMPM/Co	27	100
IZn_{50} (μM)	1	0.6
$N_S k_i$ (s^{-1})	13	35
K_{Ca} (mM) for ECa	0.7	0.35
K_{Ca}* (mM) for E*Ca	0.3	0.25
K_{Ca}*(S) (mM) (with DMPM)	0.17	0.10
K_S* for E*DTPM	0.04	0.025
K_S* for E*DTPC	0.8	0.067
K_P*(DMPM)	0.1	0.03
K_P*(DMPC)	0.03	0.02
K_I* for E*MJ33	0.0033	0.0014
XI_{50} for MJ33	0.0064	0.006
K_M*(DMPM) from K_I* and XI_{50}	1	0.4
K_M*(DMPM) from K_{Ca}*(S) and K_{Ca}*	0.9	0.67
K_M*(DMPM) from $v_o/N_S k_i$ and K_P*	0.35	0.36
k_{cat}* (s^{-1})	50	400

Table 6: Initial Rates (v_o in s^{-1}) and ICu_{50} of Hydrolysis of Phospholipid with Different Headgroups by PLA2[a]

phospholipid	v_o for Ca(II)	v_o for Co(II)	ICu_{50} (μM)
dimyristoylglycero-			
-phosphate	35	6	23
-phosphomethanol	300	100	0.5
-sulfate	40	9	40
-phosphoserine	270	35	130
-phosphoglycerol	240	138	2
-phosphocholine/DOC[b]	40	3	1.4
diheptanoylGPC	130	1	15
dioctanoylglycero-			
-phosphomethanol	1000	800	
-phosphate	340	135	
-arsonate	8	1	
-choline	600	5	

[a] Assays were carried out in the presence of 100 mM NaCl at pH 8.0 and 24 °C and 1 mM cations; the cation concentration in the presence of phosphate and phosphoserine was 0.1 mm to avoid complications due to precipitation of the lipid. The inhibition results are for the Ca cofactor. [b] DOC, 7-deoxycholate.

The Cofactor Role of Cobalt(II) Depends on the Structure of the Substrate. Hydrolysis of phosphatidylcholines is considerably slower with cobalt than with calcium (Table 6). This extends the earlier conclusion that the specificity for the *sn*-3 substituent of the substrate resides in the chemical step of the turnover cycle (*18*), and it is consistent with the observation that K_L* for phosphocholine mimics (Table 2) is 3−7-fold higher in the presence of Co(II) than in the presence of calcium. If there is a comparable change in K_M*, the rate will change at the most by a factor of 3. A more than 100-fold Ca versus Co rate difference seen with phosphatidylcholines suggests a large cation-dependent effect of the *sn*-3 substituent on k_{cat}*. In short, results in Tables 3−6 show that the cation in E*CS modulates events associated with k_{cat}*.

Calcium Remains Bound during the Chemical Step. Binding of the substrate and products to the active site of PLA2 requires calcium. Analysis of the products of the ^{18}O exchange reaction of $H_2{}^{18}O$ with E*CS or E*CP provides significant insight into the partial reactions of the chemical step, operationally dissected in Scheme 2 and Figure 2 by invoking formation and decomposition of T*. A FAB mass

Table 7: Peak (*m*/*e*) Intensities of Phospholipid Incubated with $H_2{}^{18}O$[a]

no.	lipid	E (mol %)	M^{2+}	time (min)	relative intensity (%)				
					m/*z* 227	*m*/*z* 2	*m*/*z* 4	*m*/*z* 395	*m*/*z* 605
Aa	S	0	Ca	10	67.9	0	0	28.1	100
Ab	S	0	Ca	2400	67.8	0	0	28.1	100
Ac	S	0.01	Ca	1	80.1	0	0	43.1	100
Ad	S	0.01	Ca	6	87.4	0	0	46.1	100
Ae	S	0.01	Ca	12	59	4.1	0	52.8	100
Ai	S	0.01	Ca	31	89.5	5.3	0	61.8	100
Ak	S	0.01	Ca	50	92.7	6.7	0	70.7	100
Ao	S	0.01	Ca	86	83	5.6	0	91.8	100
Av	S	0.01	Ca	185	77.7	8.2	2.0	76.9	100
Aac	S	0.01	Ca	>3000	15.5	5.4	3.8	100	0
Bf	S	0.3	Ca	1.2	41.7	10.4		100	27.2
Bg	S	0.3	Ca	7	26.2	7.3		100	10.8
Bh	S	0.3	Ca	11	35.4	12.2		100	8.5
Bj	S	0.3	Ca	22	28.4	8.3		100	6.4
Bl	S	0.3	Ca	40	33.4	9.2		100	4.7
Bn	S	0.3	Ca	58	30.3	9.9		100	2.6
Bw	S	0.3	Ca	174	23.2	7.0		100	0
Cm	S	2	Ca	2	16.5	7.2	9.2	100	0
Cr	S	2	Ca	40	16.6	6.5	12.1	100	0
Cx	S	2	Ca	135	22.8	6.4	13.4	100	0
Dp	S	2	bkg	1	28.1	15.3		100	12.5
Dt	S	2	bkg	20	14.2	4.5	8.0	100	0
Dy	S	2	bkg	110	16.0	8.2	13.7	100	0
Eq	S	2	Zn	0.1	100	7.5	0	65.1	100
Es	S	2	Zn	12	32.6	12.3	3.3	100	24.5
Eu	S	2	Zn	24	22.5	13	4.1	100	6.2
Ez	S	2	Zn	115	19.5	11.6	4.1	100	0
Eaf	S	2	Zn	180	17.5	8.9	4.3	100	0
Faa	MA	0	Ca	2	100	0		0	0
Faw	MA	0	Ca	1150	100	0		0	0
Gab	MA	2	Ca	2	100	0		0	0
Gav	MA	2	Ca	1150	100	0		0	0
Hae	MA/LPM	0	Ca	0	22.3	0		100	0
Hag	MA/LPM	0	Ca	3000	23.4	0		100	0
Has	MA/LPM	2	Ca	3000	42.5	80.4	100		
Hax	MA/LPM	2	bkg	3000	54.7	72.8	100		
Hay	MA/LPM	2	Zn	3000	100	80.7	51.6		
Jah	S	4	10Zn	0	48.8	13.6		100	76.7
Jai	S	4	10Zn	8	27.3	11.1		100	18.1
Jaj	S	4	10Zn	10	17.6	15.6		100	12.0
Jak	S	4	10Zn	12	24.7	12.9		100	4.2
Jal	S	4	10Zn	16	21.7	13.1		100	3.3
Kam	S	0.4	10Zn	0	60.8	5.5		57.9	100
Kan	S	0.4	10Zn	2	79.4	11.6		90.5	100
Kao	S	0.4	10Zn	5	70	15.1		100	79.8
Kap	S	0.4	10Zn	7	53.3	14.2		100	63.3
Kaq	S	0.4	10Zn	13	34.3	7.1		100	51.4
Kar	S	0.4	10Zn	17	42.1	10.6		100	33.4
Kat	S	0.4	10Zn	26	23	8.5		100	13.4
Kau	S	0.4	10Zn	66	18.0	7.8		100	5.7
Kay	S	0.4	10Zn	1100	17.7	9.1	2.2	100	0

[a] bkg, background level. [Ca] = 0.5 mM. [Zn] = 0.02 or 0.2 mM.

spectrum of DMPM shows the parent peak at *m*/*z* 605 and two major fragments: *m*/*z* 227 from the myristate (MA) and a *m*/*z* 395 fragment corresponding to LPM resulting from the loss of ketene from DMPM (*28*). MA alone gives the *m*/*z* 227 peak, and LPM gives *m*/*z* 395 and 227 peaks. Exchange of one or both oxygens in MA with ^{18}O gives *m*/*z* 229 and 231, respectively. Besides the relative abundance (concentration), the FAB-MS peak intensities depend on a host of factors: apparent sensitivity (LPM > MA), differing interactions with the matrix, and differing intrinsic rates for the parallel reactions which produce individual fragment ions. For these reasons, it is not possible to quantify the concentrations of the individual species from the FAB-MS results alone. However, the singly and doubly ^{18}O exchanged species of MA, which are only enzymatically produced, reflect changes in the product levels with the reaction conditions. Thus, the relative *m*/*z* 229 and 231 peak intensities are proportional to the changes in concentrations of these species with time, reaction conditions, and the ^{18}O exchange reaction.

At short incubation times (A and B in Table 7), only one O^{18} is incorporated in the initially produced myristate product (*m*/*z* 227 and 229), as also reported by Ghomaschi et al. (*31*). The O^{18}-labeled substrate (e.g., *m*/*e* 607) or lysophospholipid (*m*/*z* 397) is not detected under any of the conditions, with an upper limit of 1% for the O^{18} exchange with the substrate. These results are consistent with the mechanism in Figure 2, where the two oxygens of T*, one from the carbonyl

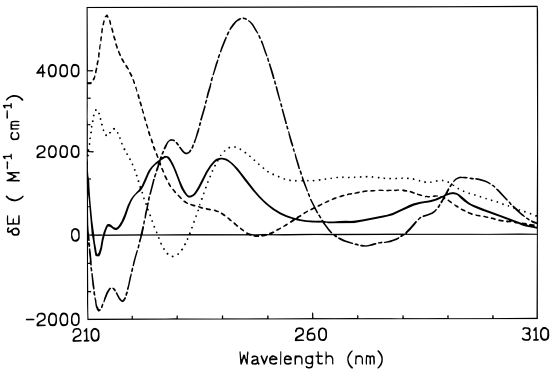

FIGURE 6: Change in the UV difference spectrum of pig pancreatic PLA2 (10 μM) in the aqueous phase (E form) induced by calcium (dots). Also shown are the difference spectra for PLA2 bound to 4.3 mM deoxy-LPC (E*) induced by calcium (—), barium (− −), and zinc (−•−). Conditions were 10 mM Tris at pH 8.0 with 1 mM Ca or Ba or 0.2 mM Zn.

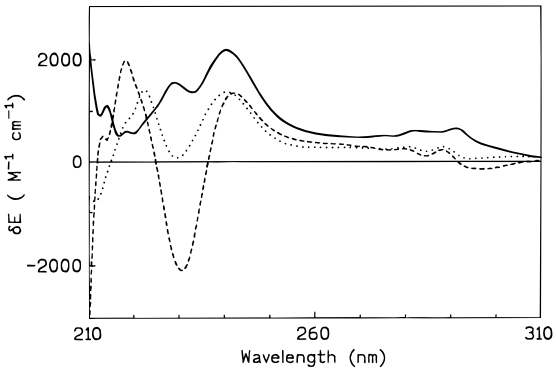

FIGURE 7: UV difference spectra induced by 1 mM calcium added to bovine pancreatic PLA2 WT (—), H48A (− −), and Y52F/Y73F (•••) bound to 4.3 mM deoxy-LPC. Other conditions were like those described in Figure 6.

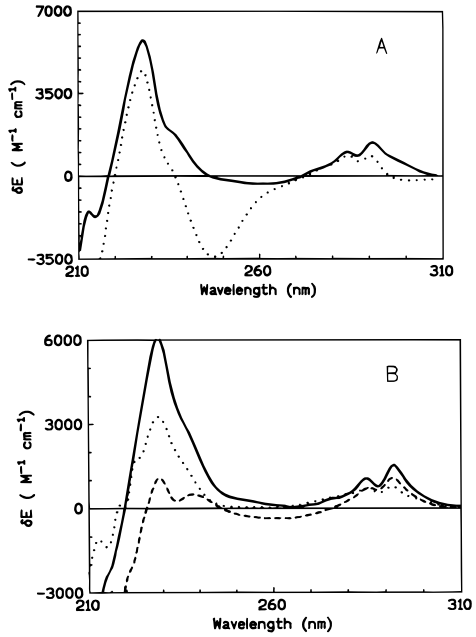

FIGURE 8: (A) UV difference spectra induced on the binding of MJ33 to pig pancreatic PLA2 bound to 4.3 mM deoxy-LPC in the presence of calcium (—) and zinc (•••). (B) UV spectral change induced by MJ33 added to bovine PLA2 WT (—), H48A (− −), or Y52F/Y73F (•••) in the presence of calcium. Other conditions were like those described in Figure 6.

oxygen and the other from the nucleophile, cannot change their positions before leaving the enzyme in the forward or the reverse direction.

At longer periods of incubation of E*Ca·DMPM (Av vs Aac), the *m*/*e* 229 intensity begins to decrease with the appearance of *m*/*z* 231 due to the exchange of the second ^{18}O in myristate. The *m*/*z* 231 peak is also seen if the reaction is carried out with E*CaP (Has and Hax in Table 7). Controls show that ^{18}O exchange in MA is seen only if both the products, as well as PLA2 and calcium, are present in the reaction mixture. The rates of appearance and disappearance of *m*/*z* 229 show a dependence on the amount of enzyme and calcium. These results show that E*CaP exchanges ^{18}O in myristate through the formation of T* (Figure 2).

The rate of hydrolysis of DMPM monitored as the change in *m*/*z* 605, 395, and 227 is considerably slower in the presence of zinc (E and J in Table 7), even slower compared to that with background calcium (D). Since the rate of hydrolysis in the presence of the background levels of calcium is significant on the time scale of these measurements, it is not possible to unequivocally ascertain whether zinc promotes hydrolysis. On the basis of the observation that in the presence of Zn the ^{18}O exchange is considerably below the background calcium level (Hey, J, and K), we suspect that E*ZnS or E*ZnP do not participate in the formation of any of the reaction intermediates required for the ^{18}O exchange from water.

UV Difference Spectral Signatures Induced by Mimics Depend on the Nature of the Cation(II). Evidence that the ground state of E*CS complexes is different for calcium and inhibitory Zn is provided by the UV absorbance of PLA2. The spectral signatures, determined as the difference spectra, result from a shift in the spectral mass and distribution; i.e., the peak positions in the difference spectra do not necessarily correspond to a change in the peak position in the absorption spectrum from a chromophore. Absorbance changes in the 210−310 nm range are induced upon the binding of cations and mimics to PLA2 (Figures 6−9). The changes in the 280−300 nm region are attributed to a change in the only tryptophan (Trp-3) present at the interfacial recognition face of PLA2. These changes are small with a molar extinction coefficient of <1000 M^{-1} cm^{-1}, and they are largely associated with the changes in the N terminus segment due to the binding of a mimic to the active site of the enzyme at the interface (*32*−*34*). The changes in the 220−250 nm region are assigned mostly to His-48. The changes are not observed with the H48A mutant, and the changes are less prominent in the Y52F/Y73F double mutant. The spatial relationship between these residues is shown in Figure 1A.

The spectral changes in the 220−250 nm region depend on the nature of the cation and the mimic in the active site. Changes induced by the binding of calcium to the E form is appreciably different from that with the E* form (Figure 6). Also, the difference spectra in E* induced by Ca, Ba, and Zn are different. The calcium-induced changes in the E* form of pig (Figure 6) and the bovine PLA2 (Figure 7) are comparable. These two enzymes differ in >20% residues; however, their architecture is virtually identical (*6*, *35*). Also as compared in Figure 7, the 230 nm region is considerably

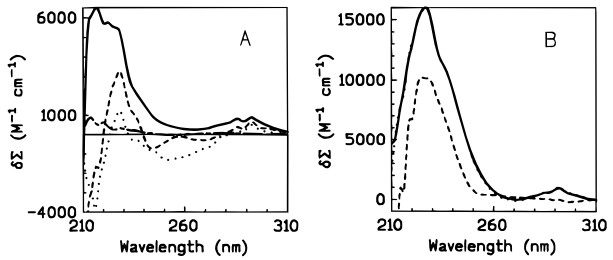

FIGURE 9: (A) UV spectral change induced by RM2 (—), MG14 (− −), MJ33 (•••), and AM3 (−•−) added to the E*Ca form of pig PLA2 on deoxy-LPC. Under these conditions, about 50% of the enzyme would be converted to the E*I form. (B) UV spectral change induced by addition of dioctanoylphosphatidylmethanol to the E* form of pig PLA2 on deoxy-LPC in the presence of calcium (—) or zinc (− −). The spectra in the presence of the substrate were taken 5 s after the addition of the substrate, and a sufficient excess is likely to be present.

depressed in the difference spectrum from the E* form of H48A, and less so with Y52F/Y73F.

Binding of MJ33 to form the ternary E*CI complex also induces a significant change in the 210−260 nm region (Figure 8). The changes induced by the binding of MJ33 to the E*Ca and E*Zn forms of pig PLA2 differ significantly in the 245 nm region with a modest difference in the 290 nm region (Figure 8A). Also, the binding of MJ33 to the E*Ca form of bovine WT or the H48A or Y52/73F mutant shows a major change near 230 nm, and a minor effect near 245 nm (Figure 8B). Differential perturbation of His-48 and Trp-3 is also induced by four competitive inhibitors (Figure 9A) and DC_8PM (Figure 9B) added to the E*Ca form of pig PLA2.

Collectively, remarkable plasticity of the active site region of PLA2 is indicated by the kinetic and binding results. UV difference spectra show that the binding of Ca or Zn to E, E*, or E*I forms of PLA2 induces characteristic spectral perturbations. Crystallographic evidence suggests that the backbone conformation is not significantly altered on the binding of the cation and the mimic; however, the headgroup of bound mimics interacts with His-48, and the chain interacts with Trp-3 (*6*−*11*). The dependence of the spectral signatures on the nature of the cation and mimic also suggests that side chains are involved in the cation and mimic binding. Among other factors, ionization, H-bonding, and tautomeric states of the imidazole ring could change with the nature of the cation and the hydrogen bonding tendencies of the functional groups on the mimic. Thus, the changes in the 230 nm region are assigned to the His-48 chromophore coupled to Tyr-52 and -73 through Asp-99 (Figure 1A). The inhibitory cations form dead-end complexes with spectroscopic signatures that suggest a change in residues connecting the catalytic His-48•Asp-99 pair to Tyr-52 and -73, and the N-terminal helix. How these interactions control the stability of the Michaelis complex and its partitioning for the chemical step remains to be determined.

DISCUSSION

Calcium regulates numerous processes in living organisms. It is found in crystal structures of several hundred proteins, where a general pattern of its coordination behavior is beginning to emerge (*36*, *37*). Yet a role of calcium as a cofactor in the catalytic turnover cycle is apparently established, to the best of our knowledge, only for α-amylase (*38*), staphylococcal nuclease (*39*, *40*), and trypanosomal nucleoside hydrolase (*41*). For the nuclease, a convincing case is made for the nucleophilic catalytic role of a water molecule in the first or second coordination sphere of calcium (*42*), where cobalt acts as a competitive inhibitor by binding in a vestibular site adjacent to the calcium site (*43*).

Results with PLA2 show a role for calcium in the substrate binding and the chemical step, and a remarkable plasticity of the active site environment is also indicated. Ca, Co, and Ni show comparable k_{cat}* values with anionic substrates, but not with zwitterionic *sn*-3-phosphatidylcholines (Table 6). We attribute such effects to differences in the coordination geometry of the cation in E*CS; i.e., only the catalytic cations favor a near-attack conformation (Figure 1B). The significance of key results related to the chemical step is discussed below in the context of the mechanism in Figure 2.

Near-Attack Conformation for Esterolysis by PLA2. PLA2-catalyzed esterolysis is $>10^{10}$-fold faster than uncatalyzed esterolysis (*44*−*46*). Within the paradigm of a nucleophilic attack (*47*, *48*), formation of a near-tetrahedral transition state or intermediate (T*) in the chemical step of PLA2 is often assumed (*3*, *4*, *6*, *10*, *49*, *50*). According to the mechanism in Figure 2, during the attack of W5 on the ester carbonyl coordinated to calcium, the His-48•Asp-99 pair accepts the proton through W6, and during the decomposition, the proton is transferred to the leaving group.

Factors favoring catalysis by enzymes involve both ground state and transition state features, including the effective pK_a of the general acid (*51*, *52*), the relative orientation and position of the reactant species (*53*−*55*), and the entropic contributions from freezing motions (*56*). In a remarkable synthesis of intramolecular catalysis, Lightstone and Bruice (*55*) have suggested that the catalytic advantage comes mainly from the near-attack ground state conformers on the way to the enthalpy-dominated factors in the transition state. In our mechanism, the movement of proton from the nucleophilic water to His-48 and then to the leaving group occurs through W6 located between Ca, δNH, and the carboxylic ester oxygens. In addition, the expanded eight-coordinate square antiprism geometry (Figure 1B) has a suitable near-attack conformation. The angle of approach of the nucleophile is within a 20° cone from the perpendicular to the ester O−C═O plane. Also, the distance between W5 and the carbonyl carbon, 3.26 Å, is nearly ideal for a nucleophilic attack (*54*, *57*). This conformation may be sufficiently activated, but not much strained, along the reaction coordinates with a minimum change in the position, orientation, or charge distribution around the cation.

Plasticity of the active site is indicated by the range of glycerophospholipid headgroups that are accommodated in the active site, and factors that stabilize the anionic character on the ester oxygens are indicated in crystal structures of PLA2 with substrate mimics. With MG14 or RM-2, calcium is seven-coordinate and the NH of Gly-30 is hydrogen bonded to the carbonyl oxygen of the substrate (*10*, *11*). In the MJ33 complex, calcium is six-coordinate and the NH of Gly-30 is H-bonded to the other oxygen on the tetrahedral phosphate; also, the OH of Tyr-69 is a short hydrogen bond (2.8 Å) away from the *sn*-2-ester oxygen, where it could stabilize a charge (*9*).

Expansion of the Cation Coordination Shell in PLA2. We propose that during the chemical step the coordination geometry of calcium(II) changes from pentagonal bipyramid to a square antiprism (Figure 1B). Calcium with eight ligands is found in α-amylase (*38*, *60*), proteinase K (*52*), and nucleoside hydrolase (*41*). A change in the coordination number from seven to eight is observed upon sugar binding to the C-type mannose binding protein (*61*). Such a change in the coordination number is permitted for the electrostatic complexes of calcium (*36*, *62*, *63*) with a small energy penalty (*37*), and the stability of complexes increases from H-bonding between ligand in the same polyhedron or the neighboring groups (*62*, *64*). Simulations (*65*; also see the Supporting Information) show that the coordination number change from seven to eight in PLA2 (Figure 1B) occurs with very favorable hydrogen-bonding relationships, and without any unfavorable steric contacts or perturbation of the protein side chains or backbone. A particularly striking feature of the coordination environment of the cation that emerges from such docking exercises is that six-coordinate octahedral and eight-coordinate antiprismatic geometries are generated from the seven-coordinate pentagonal bipyramidal geometry of calcium in PLA2 without a shift in the position of the five ligands provided by PLA2 (Figure 1B). A four-coordinate geometry, even if somewhat strained, preferred by Cd, Zn, and Cu, could be achieved if the carboxylate of Asp-49 provides a single ligand. These readily interconvertible geometries are closely related, and are preferred for the respective coordination numbers (*66*, *67*).

It is likely that 3d-cations(II) form ionic complexes with PLA2. Virtually all 3d-cations(II) with a radius of less than 1.1 Å form stable EC, E*C, and E*CL complexes. Since only five oxygen ligands are provided by the protein, differences in the partial desolvation tendencies of the cations (*71*) or the ligand substitution energies could account for some of the differences in the dissociation constants. The extent of ligand substitution associated with the formation of these complexes with Cu, Zn, or even Co for that matter is difficult to predict, and must await crystallographic results.

The ability to accommodate a range of geometries in the active site is also evident from the structural diversity of the inhibitors that compete with the substrate and bind to the active site (*24*, *68*). Such complexes of PLA2 are formed without a change in the backbone structure (*6*, *9*−*11*); however, changes in the His-48 chromophore (Figures 6−9) suggest significant changes in the side chains. The binding of inhibitors to the active site of E* is driven primarily, if not exclusively, by headgroup interactions (*15*, *22*, *24*) after the partitioning of the mimic into the interface is taken into account (*69*). This is not surprising because during the formation of the E*CaL complex at the interface the acyl chains are transferred from the hydrophobic region of the bilayer to the hydrophobic environment of the active site cavity. The importance of the headgroup interactions is emphasized further by the fact that primary acylamides, such as AM3 (Table 2), are potent calcium-dependent active site-directed inhibitors of PLA2, whereas their *N*-methyl derivatives are less potent by a factor of 50 (*22*). This is a surprising result in light of the fact that secondary acylamides, such as the *sn*-2-amidophospholipid analogues, are potent inhibitors (*70*; also see earlier papers of the series). This difference is best rationalized by invoking expanded eight-coordinate geometry (see ref *74* and the Supporting Information).

Dynamics of the Catalytic Water. With expanded coordination (Figure 1B), the carbonyl carbon is 3.4 Å from W5 and 4.1 Å from W6. Both of these potential nucleophiles are held between Ca and δNH-H48 (Figure 1B). The angle of approach of W6 (90° from the trigonal C═O plane) to the carbonyl carbon is somewhat more favorable compared to 60° for W5. W6 is a better proximal proton acceptor because it is H-bonded to H48·D99. Direct coordination of W5 to the cation makes it a stronger proton donor, and additional activation is expected because the dicationic calcium is coordinated to ligands with only one net negative charge. Also, H-bonding of W5 to the more basic electron pair of O1 (*64*, *72*) places Asp-49 in an excellent position to assist in the deprotonation of W5.

It is difficult to predict the pK_a of water coordinated to a metal ion in general terms, especially if the metal is held by structurally different ligands (*73*). The net charge and a proton from W5−W6 could be shared by the carbonyl oxygen, ester oxygen, the imidazole ring, and possibly carboxylate of D99. An effectively lower pK_a of W5−W6 is expected due to the coupling to calcium and to His-48. It is also consistent with the observation that the pK_a of His-48 decreases from 7 to 5.7 in the presence of the bound calcium, and K_{Ca} decreases from 2.5 mM at pH 6 to 0.3 mM at pH 8 (*3*).

The role of W5−W6 as the catalytic water is also suggested by molecular dynamic simulation of the ternary E*CaS complex of PLA2 (*50*). As the initial condition, only W6 was included as the "catalytic water" and W5 was substituted by the carbonyl oxygen of the substrate in the pentagonal bipyramidal geometry. During the 48 ps simulation, W6 occupied alternating positions occupied by W6 and W5. Toward the end of the simulation, W6 and another water molecule joined in the expanded coordination shell of calcium, thus making up a total of nine ligands. Since W5 was not modeled, this simulation is equivalent to a situation where two water molecules coexist in positions occupied by W5 and W6 with the carbonyl oxygen in the expanded coordination shell. In short, not only is there ample space for simultaneous placement of carbonyl oxygen, W5, and W6, but they can also be suitably placed for a nucleophilic attack without a large movement and reorientation of any of the groups involved.

Factors Controlling the Energetically Demanding Transition State. A range of effects on k_{cat}* imply a role for multiple interactions in the chemical step. Ultimately, the following observations must be accommodated in any formulation of the reaction coordinates.

(a) On the basis of the oxy/thio ratio of 10, the chemical step is rate-limiting (*29*) with k_{cat}* equal to k_2 which is 400 s^{-1} for DMPM (*14*) and about 3000 s^{-1} for DC_8PC (*15*). These effects on k_{cat}* (Table 3; also see ref *29*) are consistent with the participation of the *sn*-2-oxygen in the transition state.

(b) The $^{12}C/^{14}C$ carbonyl carbon isotope effect is 1.01 for the hydrolysis of DMPM by PLA2 (*31*). It suggests a strong commitment for catalysis without equilibration of the isotopic substrate species in E*CS, which is consistent with experimentally observed k_{-1}* ≪ k_{cat}* (*14*).

(c) D99N PLA2 is modestly (25-fold) k_{cat}*-impaired (*8*). As is the case with WT, the amide oxygen of N99 is H-bonded to ϵ-NH of His-48. Thus, a moderate effect of Asp to Asn substitution is expected on the tautomeric deprotonated δN for the proton transfer.

(d) Initial incorporation of a single ^{18}O in the myristate product, and the lack of ^{18}O exchange in the substrate, suggest formation of a species in the chemical step where the carbonyl oxygen and the one from the nucleophile do not become equivalent.

(e) The headgroup specificity of the substrate, with different *sn*-3 substituents, lies in k_{cat}*; e.g., the substrate specificity for *sn*-3-phosphate, -sulfate, or -arsonate substituents is in k_{cat}* (*18*, *30*, *58*, *59*, *76*), and not in K_S* (*22*, *24*). The charge on *pro-S* oxygen of the phosphate also plays a role in k_{cat}* because the phosphomethyl ester of DMPM binds to the active site (*24*) and the rate of hydrolysis is low (*58*).

(f) The approach of the anionic *pro-S* oxygen of the *sn*-3-phosphate to Ca is aided by the interaction of the *pro-R* oxygen with the hydroxyl of Tyr-69; however, Y69F is modestly k_{cat}*-impaired.

(g) Hydrogen bonding of the *sn*-2-OH of the lysophospholipid product is suggested by a more than 100-fold lower affinity of PLA2 for the 2-deoxy analogue, deoxy-LPC (*24*).

(h) The K_M*/K_I* ratio for tetrahedral mimics is about 100. The K_S*/K_I* ratio is about 10 because k_2* $\gg$ k_{-1}*. It implies that the *sn*-2 tetrahedral geometry does not resemble the transition state, yet a tetrahedral intermediate may be part of the chemical step.

In our formulation of the reaction mechanism (Figure 2), interactions of the substrate ester oxygen with OH of Tyr-69 and of NH of Gly-30 with the carbonyl oxygen (*9*) assist in the trigonal to tetrahedral conversion of the carbonyl carbon, and subsequent rotation around the ester C−O bond influences the glycerol backbone. Torsional rotation of the C−O−C_2(glycerol) single bond is followed by changes that require a shift in the position of atoms that result in the substitution of the apical water (W12) by the *pro-S* oxygen of the *sn*-3-phosphate. Besides depolarizing the anionic charge on the oxyanion hole, anionic phosphate could also push W12 in the position originally occupied by W5 in the first coordination shell of calcium. Although the magnitude of each of these effects is modest, the total contribution would be significant.

ACKNOWLEDGMENT

We gratefully acknowledge numerous discussions with Dr. Jenny Glusker on the coordination environment of calcium in proteins. We express appreciation for numerous insightful comments from an anonymous reviewer. We dedicate this work to Prof. Bert Verheij, who contributed so much to the field.

SUPPORTING INFORMATION AVAILABLE

Further discussion of the mechanism, a table showing the molecular dynamics parameters for acylamide docked in PLA2, and a figure showing the calculated distances for the energy-minimized coordination environment of calcium in the acitve site of PLA2 (8 pages). Ordering information is given on any current masthead page.

REFERENCES

1. de Haas, G). H., Bonsen, P. P. M., Pieterson, W. A., and Van Deenen, L. L. M. (1971) *Biochim. Biophys. Acta 239*, 252−266.
2. Verheij, H. M., Volwerk, J. J., Jansen, E. H. J. M., Puijk, W. C., Dijkstra, B. W., Drenth, J., and de Haas, G. H. (1980) *Biochemistry 19*, 743−740.
3. Verheij, H. M., Slotboom, A. J., and de Haas, G. H. (1981) *Rev. Physiol. Biochem. Pharmacol. 91*, 91−203.
4. Dijkstra, B. W., Drenth, J., and Kalk, K. H. (1981) *Nature 289*, 604−606.
5. Dijkstra, B. W., Kalk, K. H., Hol, W. G. J., and Drenth, J. (1981) *J. Mol. Biol. 147*, 97−123.
6. Scott, D., and Sigler, P. (1994) *Adv. Protein Chem. 45*, 53−88.
7. Kumar, A., Sekharudu, C., Dupureur, C. M., Zhu, H., Tsai, M. D., and Sundaralingam, M. (1994) *Protein Sci. 3*, 2073−2081.
8. Sekar, K., Yu, B.-Z., Rogers, J., Lutton, J., Liu, X., Chen, X., Tsai, M.-D., Jain, M. K., and Sundaralingam, M. (1997) *Biochemistry 36*, 3104−3114.
9. Sekar, K., Eswaramoorthy, S., Jain, M. K., and Sundaralingam, M. (1997) *Biochemistry 36*, 14186−14191.
10. Scott, D., White, S. P., Otwinowski, Z., Yuan, W., Gelb, M. H., and Sigler, P. B. (1990) *Science 250*, 1541−1546.
11. Thunnissen, M. M. G. M., Ab, E., Kalk, K. H., Drenth, J., Dijkstra, B. W., Kuipers, O. P., Dijkman, R., de Haas, G. H., and Verheij, H. M. (1990) *Nature 347*, 689−691.
12. Tsai, T. C., Hart, J., Jiang, R., Bruzik, K., and Tsai, M. D. (1985) *Biochemistry 24*, 3180−3188.
13. Yu, B.-Z., Berg, O. G., and Jain, M. K. (1993) *Biochemistry 32*, 6485−6492.
14. Berg, O. G., Yu, B.-Z., Rogers, J., and Jain, M. K. (1991) *Biochemistry 30*, 7283−7297.
15. Berg, O. G., Rogers, J., Yu, B.-Z., Yao, J., Romsted, L. S., and Jain, M. K. (1997) *Biochemistry 36*, 14512−14530.
16. Jain, M. K., Gelb, M. H., Rogers, J., and Berg, O. G. (1995) *Methods Enzymol. 249*, 567−614.
17. Li, Y., Yu, B.-Z., Zhu, H., Jain, M. K., and Tsai, M. D. (1994) *Biochemistry 33*, 14714−14722.
18. Rogers, J., Yu, B.-Z., Serves, S. V., Tsivgoulis, G. M., Sotiropoulos, D. N., Ioannou, P. V., and Jain, M. K. (1996) *Biochemistry 35*, 9375−9384.
19. Jain, M. K., Rogers, J., Jahagirdar, D. V., Marecek, J. F., and Ramirez, F. (1986) *Biochim. Biophys. Acta 860*, 435−447.
20. Jain, M. K., Maliwal, B. P., de Haas, G. H., and Slotboom, A. J. (1986) *Biochim. Biophys. Acta 860*, 448−461.
21. Jain, M. K., Rogers, J., Marecek, J. F., Ramirez, F., and Eibl, H. (1986) *Biochim. Biophys. Acta 860*, 462−474.
22. Jain, M. K., Ghomashchi, F., Yu, B. Z., Bayburt, T., Murphy, D., Houck, D., Brownell, J., Reid, J. C., Solwiej, J. E., Wong, S. M., Mocek, U., Jarrell, R., Sasser, M., and Gelb, M. H. (1992) *J. Med. Chem. 35*, 3584−3586.
23. Jain, M. K., Yu, B.-Z., Rogers, J., Ranadive, G. N., and Berg, O. G. (1991) *Biochemistry 30*, 7306−7317.
24. Jain, M. K., Tao, W., Rogers, J., Arenson, C., Eibl, H., and Yu, B.-Z. (1991) *Biochemistry 30*, 10256−10268.
25. Jain, M. K., Rogers, J., Berg, O. G., and Gelb, M. H. (1991) *Biochemistry 30*, 7340−7348.
26. Cajal, Y., Rogers, J., Berg, O. G., and Jain, M. K. (1996) *Biochemistry 35*, 299−308.
27. . Tsien, R., and Pozzan, T. (1989) *Methods Enzymol. 172*, 230−262.
28. Murphy, R. C., and Harrison, K. A. (1994) *Mass Spectrom. Rev. 13*, 57−75.
29. Jain, M. K., Rogers, J., Gelb, M. G., Tsai, M.-D., Hendrickson, E. K., and Hendrickson, S. (1992) *Biochemistry 31*, 7841−7847.
30. Cleland, W. W., and Kreevoy, M. M. (1994) *Science 264*, 1887−1890.
31. Ghomashchi, F., O'Hare, T., Clary, D., and Gelb, M. H. (1991) *Biochemistry 30*, 7298−7305.

32. Dupureur, C. M., Yu, B.-Z., Jain, M. K., Noel, J. P., Deng, T., Li, Y., Byeon, I. L., and Tsai, M. D. (1992) *Biochemistry 31*, 6402−6413.
33. Dupureur, C. M., Yu, B.-Z., Mamone, J. A., Jain, M. K., and Tsai, M. D. (1992) *Biochemistry 31*, 10576−10583.
34. Jain, M. K., and Maliwal, B. P. (1993) *Biochemistry 32*, 11838−11846.
35. Dijkstra, B. W., Renetseder, R., Kalk, K. H., Hol, W. G. J., and Drenth, J. (1983) *J. Mol. Biol. 168*, 163−179.
36. McPhalan, C. A., Strynadka, N. C. J., and James, M. N. G. (1991) *Adv. Protein Chem. 42*, 77−144.
37. Katz, A. K., Glusker, J. P., Beebe, S. A., and Bock, C. W. (1996) *J. Am. Chem. Soc. 118*, 5752−5763.
38. Boel, E., Brady, L., Brzozowski, A. M., Derewenda, Z., Dodson, G. G., Jensen, V. J., Petersen, S. B., Swift, H., Thim, L., and Woldike, H. F. (1990) *Biochemistry 29*, 6244−6249.
39. Serpersu, E. H., Shortle, D., and Mildvan, A. S. (1986) *Biochemistry 25*, 68−77.
40. Serpersu, E. H., Shortle, D., and Mildvan, A. S. (1987) *Biochemistry 26*, 1289−1300.
41. Degano, M., Almo, S. C., Sacchettini, J. C., and Schramm, V. L. (1998) *Biochemistry 37*, 6277−6285.
42. Weber, D. J., Libson, A. M., Gittis, A. G., Lebowitz, M. S., and Mildvan, A. S. (1994) *Biochemistry 33*, 8017−8028.
43. Loll, P. J., Quirk, S., Lattman, E. E., and Gravito, R. M. (1995) *Biochemistry 34*, 4316−4324.
44. Bruice, T. C., and Benkovic, S. J. (1966) *Bioorganic Mechanisms*, Vol. 1, W. A. Benjamin, Inc., New York.
45. Guthrie, J. P. (1983) *Acc. Chem. Res. 16*, 122−129.
46. Guthrie, J. P., and Cullimore, P. A. (1980) *Can. J. Chem. 58*, 1281.
47. Kirsch, J. F., and Jencks, W. P. (1964) *J. Am. Chem. Soc. 86*, 837−843.
48. Johnson, S. L. (1967) *Adv. Phys. Org. Chem. 5*, 237−330.
49. Waszkowycs, B., Hiller, I. H., Gensmatel, N., and Polying, D. W. (1990) *J. Chem. Soc., Perkin Trans. 2*, 1259−1268.
50. Jones, S. T., Ahlstram, P., Berendsen, H. J. C., and Pickersgill, R. W. (1993) *Biochim. Biophys. Acta 1162*, 135−142.
51. Gerlt, J. A., and Gassman, P. G. (1993) *Biochemistry 32*, 11943−11952.
52. Bajorath, J., Hinrichs, W., and Sanger, W. (1988) *Eur. J. Biochem. 176*, 441−447.
53. Bruice, T. C. (1976) *Annu. Rev. Biochem. 45*, 331.
54. Lighthouse, F. C., and Bruice, T. C. (1996) *J. Am. Chem. Soc. 118*, 2595−2605.
55. Lighthouse, F. C., and Bruice, T. C. (1997) *J. Am. Chem. Soc. 119*, 9103−9113.
56. Page, M. I., and Jencks, W. P. (1971) *Proc. Natl. Acad Sci. U.S.A. 68*, 1678.
57. Burgi, H. B., and Dunitz, J. D. (1983) *Acc. Chem. Res. 16*, 153−161.
58. Kuipers, O. P., Vincent, M., Brochon, J., Verheij, H. M., de Haas, G. H., and Gallay, J. (1991) *Biochemistry 30*, 8771−8785.
59. Bonsen, P. P. M., de Haas, G. H., Pieterson, W. A., and Van Deenen, L. L. M. (1972) *Biochim. Biophys. Acta 270*, 364−382.
60. Qian, M., Haser, R., and Payan, F. (1993) *J. Mol. Biol. 231*, 785.
61. Weis, W. I., Drickamer, K., and Hendrickson, W. A. (1992) *Nature 360*, 127−134.
62. Glusker, J. P. (1991) *Adv. Protein Chem. 42*, 1−76.
63. Villafranca, J. J., and Nowak, T. (1992) *Enzymes 20*, 63−94.
64. Glusker, J. P. (1995) *Acta Crystallogr. D51*, 418−427.
65. Seshadri, K., Vishveshwara, S., and Jain, M. K. (1994) *Proc. Ind. Acad. Sci. 106*, 1177−1189.
66. Kepert, D. L. (1978) *Prog. Inorg. Chem. 24*, 179−249.
67. Kepert, D. L. (1979) *Prog. Inorg. Chem. 25*, 41−144.
68. Gelb, M. H., Jain, M. K., and Berg, O. G. (1994) *FASEB J. 8*, 916−924.
69. Jain, M. K., Yu, B.-Z., and Berg, O. G. (1993) *Biochemistry 32*, 11319−11329.
70. de Haas, G. H., Dijkman, R., Lugtigheid, R. B., Dakker, N., Van den Berg, L., Egmond, M. R., and Verheij, H. M. (1993) *Biochim. Biophys. Acta 1167*, 281−288.
71. Frey, C. M., and Stuehr, J. (1974) in *Metal Ions in Biological Systems* (Sigel, H., Ed.) Vol. 1, p 69, Mercel Dekker, Inc., New York.
72. Gandour, R. D. (1981) *Bioorg. Chem. 10*, 169−176.
73. Tsubouchi, A., and Bruice, T. C. (1995) *J. Am. Chem. Soc. 117*, 7399−7411.
74. Huheey, J. E. (1983) *Inorganic Chemistry*, 3rd ed., pp 73−76, Harper & Row, New York.
75. Shannon, R. D. (1976) *Acta Crystallogr. A32*, 751−767.
76. Kuipers, P., Dekker, N., Verheij, H. M., and de Haas, G. H. (1990) *Biochemistry 29*, 6094−6102.

BI9728607